



Research article

Facile green synthesis of silver nanoparticles derived from the medicinal plant *Clerodendrum serratum* and its biological activity against *Mycobacterium* species

Vidyasagar^{a,1}, Ritu Raj Patel^{a,1}, Sudhir Kumar Singh^c, Deepa Dehari^b, Gopal Nath^c, Meenakshi Singh^{a,*}

^a Department of Medicinal Chemistry, Faculty of Ayurveda, Institute of Medical Sciences, Banaras Hindu University, Varanasi, 221005, India

^b Department of Pharmaceutical Engineering and Technology, Indian Institute of Technology (Banaras Hindu University), Varanasi, Uttar Pradesh, 221005, India

^c Department of Microbiology, Institute of Medical Sciences, Banaras Hindu University, Varanasi, 221005, India

ARTICLE INFO

Keywords:

Clerodendrum serratum

Silver nanoparticles (AgNPs)

Polyethylene glycol encapsulated silver nanoparticles (PEG-AgNPs)

Mycobacterium species

ABSTRACT

The emergence of multidrug-resistant mycobacterial strains is a significant crisis that has led to higher treatment failure rates and more toxic and expensive medications for tuberculosis (TB). The urgent need to develop novel therapeutics has galvanized research interest towards developing alternative antimicrobials such as silver nanoparticles (AgNPs). The current study focused on the anti-mycobacterial activity of green-synthesized AgNPs and its polyethylene glycol encapsulated derivative (PEG-AgNPs) with improved stability using the leaves extract of *Clerodendrum serratum*. Different characterization methods were used to analyze them. DLS analysis revealed a lower polydispersity index of PEG-AgNPs, suggesting a more uniform size distribution than that of AgNPs. The HR-TEM results revealed that the AgNPs and PEG-AgNPs have predominantly spherical shapes in the size range of 9–35 nm and 15–60 nm, respectively, while positive values of Zeta potential indicate their stability. FTIR-ATR analysis confirmed the presence of functional groups responsible for reducing and capping the bio-reduced AgNPs, whereas the XRD data established its crystalline nature. Impressively, the PEG-AgNPs exhibited maximum inhibitory activity against different Tubercular and Non-Tuberculous *Mycobacterium* species *i.e.*, *Mycobacterium smegmatis*, *Mycobacterium fortuitum* and *Mycobacterium marinum*, relative to those of AgNPs and Linezolid. The flow cytometry assay showed that the anti-mycobacterial action was mediated by an increase in cell wall permeability. Notably, the results of AFM confirm their ability to inhibit mycobacterial biofilm significantly. We demonstrated the nontoxic nature of these AgNPs, explicated by the absence of hemolytic activity against human RBCs. Overall, the results suggest that PEG-AgNPs could offer a novel therapeutic approach with potential anti-mycobacterial activity and can overcome the limitations of existing TB therapies.

* Corresponding author.

E-mail address: meenakshisingh@bhu.ac.in (M. Singh).

¹ Contributed equally.

1. Introduction

The genus *Mycobacterium* includes over 190 species within the Actinomycetota phylum and is classified under its own family, Mycobacteriaceae. Mycobacteriaceae encompass *Mycobacterium tuberculosis* complex (MTBC) causing tuberculosis (TB) and Non-Tuberculous Mycobacteria (NTM), known for opportunistic infections [1]. MTBC includes *Mycobacterium tuberculosis* (Mtb), *Mycobacterium africanum*, *M. bovis*, etc. causing ~10.4 million TB cases yearly [2]. Among NTMs, *Mycobacterium fortuitum*, *M. chelonae*, and *M. abscessus* are prevalent rapidly growing mycobacteria (RGM) causing extrapulmonary infections, notably in those with pre-existing lung conditions [3]. *M. fortuitum* can cause skin, bone, joint, and eye infections, often nosocomial and treated with antibacterial agents like amikacin, imipenem, and moxifloxacin [4]. In addition, *M. marinum*, a slow-growing NTM, causes TB-like infections in fish and skin lesions in humans, including rare disseminated instances in HIV/AIDS patients [5]. TB caused by MTBC is a communicable disease that mainly affects the lungs. It spreads from infected to healthy individuals through the inhalation of tiny air droplets released into the air while coughing or sneezing. More people have died from TB than any other infectious disease in the past 2000 years. TB was the main infectious disease killer in the globe up until the SARS-CoV-2 outbreak. TB alone caused 1.6 million deaths worldwide in 2021 [6]. The COVID-19 pandemic emerged in India in December of 2019, overloading the healthcare system and possibly affecting the diagnosis and treatment of TB cases, undoing recent progress towards the elimination of TB by 2025 [7]. With a lengthy chemotherapy course lasting at least 6 months, TB can be cured and treated. But now it has become a serious worldwide health issue mostly due to the rapid rise in DR/MDR/XDR (Drug-/Multidrug-/Extensively drug-resistant) mycobacterial strains found to be resistant to isoniazid and rifampicin [8]. Therefore, the four anti-TB first-line medications recommended *i.e.*, isoniazid, rifampicin, ethambutol, and pyrazinamide are proving to be inefficient against DR/MDR/XDR mycobacterial strains. Recent drug abuse in the COVID-19 pandemic has only contributed to the elevated mycobacterial drug resistance in the TB-infected individuals that has led to higher treatment failure rates, and more toxic and expensive medications. In addition to this, mycobacterial species have also adapted to thrive in hostile conditions, by self-assembling into highly organized, surface-attached, and matrix-encapsulated structures known as biofilms. The biofilm consists of a thick and waxy cell wall rich in arabinogalactan and mycolic acid. The MTBC has been hypothesized to form biofilm inside the lungs of infected individuals and evade the host immune system resulting in long-term persistence [9]. The World Health Organization (WHO) has called for immediate action in the development of highly effective and novel drugs [10] to tackle the current anti-mycobacterial drug crisis, and instantaneously reverse this grave situation. However, despite the enormous efforts in drug development and generation of newer anti-TB drug regimens [11] and pipelines, only a handful of them make it to the clinical trial phase for various reasons *i.e.*, poor bioavailability, adverse drug reactions, toxicity, and elevated enzyme levels. Therefore, the need of the hour is the discovery of novel effective drugs [12] that are safe, more stable, gets easily absorbed and metabolized within the patient's body. Recently, the advent of nanotechnology vastly contributed to the treatment of chronic human diseases including TB, through the targeted and site-specific administration of precise drugs [13].

Nanotechnology is one of the most emerging and promising technologies of this century with vast applications about human health. It refers to the study of nanoparticles with sizes usually ranging between 1 and 100 nm [14]. A fascinating area of nanotechnology is the use of nanoparticles in human healthcare and medicine. Since metallic nanoparticles are similar in size to biomolecules; they have been actively explored in recent years for their potential as medicines [15]. The properties of Nano-materials can be changed depending on their shape, size way of preparation, nature of metals, and use of capping or encapsulating agents [16]. Nanoparticles can interact with pathogenic bacteria effectively because of their high surface-to-volume ratios, and they are also helpful in the drug delivery process [17]. Nanomedicine can be used to administer therapeutic substances in a controlled manner to specific targeted locations. Among several metals used for the synthesis of nanoparticles, silver is of greater interest because of its strong and broad-spectrum anti-bacterial properties. This has contributed to the extensive use of AgNPs against drug-resistant strains of bacteria. They are also reported to have anti-viral, anti-fungal, anti-inflammatory as well as anti-biofilm properties [18]. With the evolution of drug resistance, the use of Silver nanoparticles (AgNPs) against DR/MDR/XDR strains of TB can be a great alternative in disease treatment because of better and specific drug delivery [19].

However, there is always a problem with the desired size of nanoparticles for which some polymers like polyvinyl pyrrolidone (PVP) [20] and polyethylene glycol (PEG) [21], etc. are used to encapsulate them to fix particle size. Some plants act as both reducing and capping agents giving stability to the synthesized nanoparticles. Seeing an economically viable, easy, and eco-friendly method of preparation, green-synthesis emerged as more suitable among other methods like physical or chemical methods [22]. With the expanding significance of nanotechnology in healthcare and medicine, the introduction of chemically engineered nanoparticles in therapies is concerning due to potential toxic effects [23]. Therefore, non-toxic novel techniques in the field of nano research have been discovered that utilize microorganisms and plants for the synthesis of nanoparticles. In the case of green methods, the sources used for the reduction of metal salts are fungi, bacteria, algae, seaweed, and plant parts [24]. A green method is slow but has some economic benefits as it has no requirement for temperature, high pressure, or high energy [25]. In comparison to chemical and physical methods, biological processes *i.e.*, green-synthesis or phytosynthesis of AgNPs carried out using medicinal plants, offer advantages since they are biocompatible, stable, antimicrobial, more cost-effective, environment friendly, and easily accessible.

Herbal plants have been used for many years as a source of novel therapeutically active compounds, scaffolds, and pharmacophores. The WHO estimated that between 65 % and 80 % of the populations of developing nations already use medicinal plants as treatments since they are the best source for obtaining a wide range of bioactive compounds [26]. It is estimated that only 15 % of the 300,000 plant species that exist in the world have had their pharmacological potential assessed, making them a biological treasure that needs to be explored in the field of drug discovery [27].

One such target is the genus *Clerodendrum* belonging to the family Lamiaceae, which was first described by Linnaeus in 1753. The genus is diverse with about 580 species of shrubs, trees, and herbs widely distributed throughout the subtropical and tropical regions of

the biosphere [28]. The plant *Clerodendrum serratum* is commonly known as Blue Glory, Glory Bower, or Beetle Killer. *C. serratum* is a perennial woody shrub found in Sri Lanka, Malaysia, and eastern India. In several Asian nations, the species has been considered an ethnomedicinally important plant for its use to cure a variety of human diseases like asthma and rheumatism. *C. serratum* is mentioned in numerous Ayurvedic scriptures, including 'Samhitas' and 'Nighantu' for its efficacy in treating *Swasa* and *Kapha* (respiratory diseases) [29]. In this study, we have selected *C. serratum* plant for our investigation based on its promising history as a significant medicinal plant. Plant biomolecules like proteins, phenols, and flavonoids influence ion reduction and can aid in the production of stable and biocompatible metal nanoparticles. The strong anti-bacterial properties of green-synthesized AgNPs are well documented. However, not much scientific research has been carried out on the synthesis of AgNPs using the *C. serratum* plant and its anti-bacterial properties. The antimicrobial activity of green-synthesized AgNPs from *C. serratum* was established against human pathogenic bacteria *i.e.*, *Staphylococcus aureus* and *Escherichia coli* [30] whereas anti-proliferative property was demonstrated against Ehrlich ascites carcinoma (EAC) cells using cell viability and MTT assays [31]. Despite these progresses, no work has been reported on the anti-mycobacterial and anti-biofilm activities of AgNPs and polyethylene glycol encapsulated AgNPs (PEG-AgNPs) synthesized using extract of *C. serratum* against any *Mycobacterium* species till now.

Early attempts to screen drugs for TB treatment were unproductive due to the use of slow-growing Mtb. *M. smegmatis*, a fast-growing non-pathogenic species within the *Mycobacterium* genus, became an ideal model organism for mycobacterial research when the mc²155 mutant was discovered in 1990. Unlike classical models such as *Escherichia coli*, which lack genetic conservation and relevant physiology, *M. smegmatis* shares genetic orthologs and cell architecture with pathogenic mycobacteria like Mtb. Its transformability with episomal plasmids facilitated genetic studies previously impossible in slow-growing relatives. Importantly, TB drugs like isoniazid and ethambutol are effective against *M. smegmatis* but not *E. coli*, aiding in the identification of their targets. Bedaquiline, a novel TB drug, was also discovered through *M. smegmatis* screening [32]. Thus, *M. smegmatis* serves not only as a model for Mtb but for all *Mycobacterium* species and related genera, offering invaluable insights and drug discovery opportunities. Much like Mtb, *M. marinum* exhibits pathogenicity within macrophages, causing a chronic, systemic disease that resembles TB in ectotherms. Moreover, being the closest genetic relative of the MTBC, *M. marinum* serves as another ideal alternative model for research purposes [33]. Therefore, this study utilizes *M. smegmatis* and *M. marinum* as a surrogate for Mtb and evaluates the potency of AgNPs and PEG-AgNPs with *C. serratum* extract against both Tubercular and Non-Tuberculous Mycobacteria *viz.*, *M. smegmatis*, *M. fortuitum* and *M. marinum*.

The current study is the first and foremost report deciphering the synthesis and characterization of AgNPs and PEG-AgNPs using *C. serratum* extract and evaluation of their anti-mycobacterial and anti-biofilm activities against three *Mycobacterium* species.

2. Experimental

The Silver nitrate (AgNO₃) was purchased from Merck Life Science Pvt, Ltd (Grade; ACS, ISO, Reag. Ph Eur) and Polyethylene glycol 4000 from Sigma Aldrich. HPLC grade solvents *i.e.*, water (Qualigens), methanol (SDFCL), acetonitrile (SRL), and orthophosphoric acid (Sigma) were purchased from different manufacturers. The chemicals used for the culture of *Mycobacterium* species and the anti-mycobacterial activities were purchased from Himedia and were of molecular biology grade (MB).

2.1. Selection of plant

Fresh leaves of *C. serratum* were collected from the Department of Dravyaguna, Faculty of Ayurveda, Banaras Hindu University (BHU), Varanasi, India. The leaves were washed thoroughly with distilled water. It was dried at room temperature and crushed into small pieces then kept at room temperature for further use. A sample specimen was deposited at the Department of Botany, Faculty of Science, BHU.

2.2. Plant leaves extract preparation

Plant leaves were dried and crushed then 5 g of dried leaves were dissolved in 50 mL of distilled water in Erlenmeyer flask and boiled for 30 min. The mixture was filtered through Whatman filter paper and the filtrate was heated at a gentle temperature to reduce its volume by half to get concentrated plant leaves extract (PLE).

2.3. Green-synthesis of silver nanoparticles

50 mL of 1 mM AgNO₃ solution was prepared in distilled water. 5 mL of PLE was added to 45 mL of 1 mM AgNO₃ in a conical flask and stirred for 30 min at room temperature and color change was observed. Afterward, the AgNPs reaction mixture was centrifuged at 5000 rpm for 30 min using a Thermo Scientific centrifuge (Sorvall ST 8R) and the supernatant was discarded. The obtained pellets were washed thrice using centrifugation in 10 mL distilled water. Finally, the pellets were resuspended into 5 mL of distilled water. Furthered, different optimization conditions were employed to synthesize different sizes of AgNPs as mentioned below. The LabMan Probe sonicator was used to break aggregated particles at an amplitude of 25 % for 5–10 min during the optimization. Three different optimization methods were used and a total of nine AgNPs of different sizes were prepared by varying PLE/AgNO₃ concentration ratio, incubation time, and sonication time of the AgNPs reaction mixture. The methods are, a) The samples were prepared by mixing 5 mL of PLE with 45 mL of 1 mM AgNO₃ solution with varying sonication time, b) The samples were prepared by varying ratios of PLE and AgNO₃ solution taking whole volume of 50 mL and all were sonicated for 10 min each, c) The samples were prepared by increasing

incubation times of reaction mixture of AgNPs in dark from 1 to 6 h and all were sonicated for 10 min each.

For PEGylation of AgNPs, 0.5 g of polyethylene glycol (PEG) polymer was taken into 5 mL distilled water in 50 mL of the conical flask and stirred for 24 h. Then this solution was poured into 50 mL of synthesized AgNPs solution and further stirred for 48 h to get PEG-AgNPs.

2.4. Characterization of synthesized AgNPs

2.4.1. Ultraviolet–visible spectroscopy

The reduction of silver ions to nanoparticles was seen by monitoring the UV–Vis spectra of solutions after diluting the sample 10 times with ultrapure water. UV–Vis spectrophotometer (Shimadzu, UV-1800) was used to monitor the spectra of AgNP solutions from 200 to 800 nm using a quartz cuvette. To change the baseline, ultrapure water was utilized as a blank [34].

2.4.2. Zeta potential

The Zeta potential of all the formulations was analyzed by Dynamic Light Scattering (DLS) (Zetasizer, Nano-S90, Malvern) at room temperature. By using purified distilled water, nano-formulations were diluted up to four times and then passed through a 0.22 μm syringe filter (Millipore). The zeta potential of the samples was measured based on the principle of electrophoretic mobility properties of nanoparticles when placed in the electric field [35].

2.4.3. Particle size determination

The prepared formulations were optimized based on critical factors, sonication time, reaction time, and concentration of reducing agent (extract) with the response of parameters like particle size, and polydispersity index (PDI). The prepared AgNPs were diluted thrice with Milli Q water and analyzed by using Malvern Nano 3600 Zetasizer [36]. The PDI scale was analyzed for the prepared AgNPs with a 0–1 scale with 0 being monodisperse and 1 being polydisperse.

2.4.4. HPLC analysis

The analysis of phytoconstituents was carried out using the Shimadzu HPLC system (Model No. Dionex Ultimate 3000) at the Interdisciplinary School of Life Science (ISLS), BHU. The PLE, AgNPs, and PEG-AgNPs were dissolved in HPLC grade solvents and were filtered via syringe filters (0.22 μm), and the separation was performed using C18 column (15 cm \times 4.6 mm dimension) at wavelength 352 nm and 220 nm. For Reverse phase analysis, the mobile phase was prepared from HPLC-grade solvents. The chromatographic separation was performed in isocratic elution of mobile phase in the ratio of 200:100:0.75:0.75:200 of methanol: acetonitrile: acetic acid: orthophosphoric acid: water with an injection volume of 20 μl and flow rate of 1 mL/min.

2.4.5. FTIR-ATR analysis

The diverse functional groups on silver nanoparticles were analyzed by the FTIR-ATR (attenuated total reflectance) method [34, 37]. The prepared AgNPs and adjuvants compatibility study was performed by FTIR spectroscopy (Bruker-FTIR-ATR spectrophotometer, Germany).

2.4.6. Crystallographic analysis of AgNPs

X-ray diffraction (XRD) is an analysis tool that has been used to analyze crystal or polycrystalline structures, quantify chemical compound resolution, qualitatively identify diverse analytes, measure the degree of crystallinity, particle sizes, and so on. The crystalline nature of AgNPs was confirmed by the XRD pattern obtained from the Rigaku-MiniFlex 600 Desktop X-ray diffraction system, Rigaku Corporation at 2θ range from 0 to 80° , and it's compared with pure AgNO_3 and physical mixture. The nature of PLE was also analyzed. XRD sample of nano formulations concentrated solution was coated in a glass slide thrice and overnight dried at room temperature [38]. The pattern was recorded by Cu-K α radiation with λ of 1.5406 \AA at a voltage of 40 kV and current of 15 mA with a scan rate of $5^\circ/\text{minute}$.

2.4.7. HR-TEM (high-resolution transmission electron microscopy)

HR-TEM, Tecnai G2 20 TWIN, FEI Company of USA (S.E.A.) Pte, Ltd. was used to analyze the surface architecture, morphology, and size analysis of colloidal silver nano-formulations. The nanoparticle formulations were sonicated for 2 min after being diluted 5 times with ultra-pure water. One drop of each diluted sample was dropped on the TEM grids (400 mesh size) and dried under vacuum overnight before being examined by TEM [38,39].

2.5. Biological activity of synthesized AgNPs

2.5.1. Mycobacterial culture preparation

The culture of all three mycobacterial species i.e., *M. marinum* (ATCC 2275), *M. fortuitum* (ATCC 6841), and *M. smegmatis* (mc²155) were obtained from the Virus Research and Diagnostic Laboratory of Institute of Medical Sciences, BHU. All three mycobacterial species were cultured and maintained using Middlebrook 7H10 agar (solid medium) supplemented with 0.4 % (v/v) glycerol and 5 % ADC (Acid-Dextrose-Catalase) and Middlebrook 7H9 broth liquid medium supplemented with glycerol (0.4 %, v/v), Tween-80 (0.05 %, v/v) and 5 % ADC.

2.5.2. Agar disk diffusion method

The anti-mycobacterial activity of *C. serratum* PLE, AgNPs, PEG-AgNPs, AgNO₃, and Linezolid (positive control) was evaluated against *M. smegmatis*, *M. fortuitum*, and *M. marinum* through agar disk diffusion method [40,41]. Fresh streaked cultures of *Mycobacterium* species were suspended in autoclaved normal saline (0.85 %) and turbidity adjusted to 0.5 MacFarland (10⁵ colony-forming units per milliliter). *Mycobacterium* inoculums were spread on Middlebrook 7H10 agar plates through sterile cotton swabs and incubated for 30 min at 37 °C for *M. smegmatis* and *M. fortuitum* and 30 °C for *M. marinum*. Whatman no. 1 filter paper disks (6 mm in diameter) were placed on inoculated agar plates and 10 µl of each test compound along with positive control were impregnated on paper disks. The plates inoculated with *M. smegmatis* and *M. fortuitum* were incubated for 2 days at 37 °C and that of *M. marinum* for 3 days at 30 °C. The plates were observed for the zone of inhibition and diameters were measured. The tests were performed in triplicates and the mean diameters of the zone of inhibition were calculated.

2.5.3. Biofilm forming potential

The ability of *Mycobacterium* species to form biofilm was quantitatively analyzed using the microtitre plate method [42,43]. Overnight grown cultures of *Mycobacterium* species of 0.5 McFarland were 1:100 diluted in biofilm growth medium *i.e.*, Sauton's medium and 100 µl diluted culture of each species were dispensed in 96-well flat bottom microtitre plate (Sigma-Aldrich). A well with 200 µl media (blank), was used as negative control. The plates were sealed with parafilm and incubated at respective temperatures *i.e.*, *M. smegmatis* and *M. fortuitum* at 37 °C and *M. marinum* at 30 °C for 4 days and media was added under sterile conditions if required. After incubation, the media was aspirated out and washed with PBS thrice. The contents of the wells were fixed with 200 µl sodium acetate (2 %) incubated for 30 min and washed again with PBS thrice. Afterward, each well was then stained by adding 175 µl of a 0.5 % Crystal Violet (w/v) solution and incubated for 20 min. Further, the wells were rinsed with fresh tap water and allowed to air dry. Subsequently, stained wells were then treated with 175 µl of 95 % ethanol, and the plates were incubated at room temperature for 30 min. Finally, the optical densities (OD) were measured at 570 nm using a spectrophotometer (Thermo Scientific Multiskan FC). The experiments were performed in triplicate.

2.5.4. Biofilm formation inhibition assay

The biofilm formation inhibition potential of the compounds was evaluated against *M. smegmatis*, *M. fortuitum*, and *M. marinum* cultures using crystal violet (CV) assay [44]. The fresh cultures of *Mycobacterium* species were inoculated in a broth medium. After the turbidity reached 0.5 McFarland, 100 µl of bacterial culture (1:100 diluted) were inoculated to the wells of a 96-well microtitre plate for seeding and incubated at the respective optimum temperature for 3 days. Further, an equal volume of test compounds was added to the wells, including Linezolid and Triton X-100 as a positive control, and cultures without any test compound were taken as a negative control. The microtitre plates were sealed properly and incubated at respective temperatures *i.e.*, *M. smegmatis* and *M. fortuitum* at 37 °C and *M. marinum* at 30 °C for 4 days. The contents from the wells were decanted after incubation and washed with PBS thrice. The remaining contents of the wells were fixed with 200 µl sodium acetate (2 %) incubated for 30 min and washed again with PBS thrice. Afterward, each well was then stained by adding 175 µl of a 0.5 % Crystal Violet (w/v) solution and incubated for 20 min. Further, the wells were rinsed with fresh tap water and allowed to air dry. Subsequently, stained wells were then treated with 175 µl of 95 % ethanol, and the plates were incubated at room temperature for 30 min. Finally, the optical densities (OD) were measured at 570 nm using a spectrophotometer (Thermo Scientific Multiskan FC). The experiments were performed in triplicate.

2.5.5. Determination of minimum inhibitory concentration (MIC)

Micro broth dilution method was used to determine the minimum inhibitory concentration (MIC) of the test compounds, according to NCCLS guidelines document M27-A [45]. The lowest concentration at which a substance entirely prevents the visible growth of microorganisms in liquid media is known as its MIC value. Briefly, all three *Mycobacterium* species cultures were inoculated in 10 mL Middlebrook 7H9 broth and incubated at respective temperatures *i.e.*, *M. smegmatis* and *M. fortuitum* at 37 °C and *M. marinum* at 30 °C. Simultaneously, 500 mg/mL stock solution of PLE, 100 µg/mL of AgNPs, PEG-AgNPs, and Linezolid were prepared, and an equal volume of test compounds were mixed with culture broth which was serially two-fold diluted in each well of a 96-well microtitre plate. Subsequently, 10 µl of actively dividing bacterial cells were inoculated in each well and the plates were incubated for 24 h. The plates were observed for visible turbidity in each well and results were evaluated by measuring the optical densities (OD) at 570 nm using a spectrophotometer (Thermo Scientific Multiskan FC). All the tests were performed in triplicate and the average was considered as final MIC value.

2.5.6. Hemolytic activity

The toxicity of test compounds on human red blood cells was evaluated on blood agar plates [46]. Briefly, 5 mL of blood was drawn from a healthy individual using a sterile syringe and aseptically mixed with 95 mL of autoclaved nutrient agar medium. Once the plates were prepared, filter paper disks (6 mm in diameter) were placed and loaded with 10 µL of each test sample and control. The plates of *M. smegmatis* and *M. fortuitum* were then incubated at 37 °C and *M. marinum* at 30 °C and were observed for hemolysis after 48 h.

2.5.7. Flow cytometry analysis

To evaluate the membrane damage of *M. smegmatis*, *M. fortuitum*, and *M. marinum* treated with test compounds, FACS (fluorescence-assisted cell cytometer) analysis was performed using DNA binding dye, propidium iodide (PI) [47]. The cells at the exponential phase of 0.5 MacFarland were inoculated with growth medium in 96 well plates along with test samples. The treated cells were then transferred from wells to eppendorf tubes and centrifuged at 200 g for 5 min at room temperature. The supernatant was discarded and

cells were washed twice with PBS. The harvested cells were incubated with PI at 4 °C for 30 min in the dark. The unbound dye was removed and was re-suspended in PBS buffer. The cells were analyzed using flow cytometry (BD FACSAria™ Fusion) with excitation and emission wavelengths at 488 nm and 620 nm, respectively [48].

2.5.8. Atomic force microscopy (AFM)

For the AFM, the method of Chatterjee et al. was followed with a few modifications [49]. The biofilm samples of *M. smegmatis*, *M. fortuitum*, and *M. marinum* for AFM were prepared using glass coverslips of 11 mm diameter. The autoclaved coverslips were submerged in a 24-well polystyrene plate containing growth media in sterile conditions. Overnight-grown planktonic cultures were adjusted to 10⁶ cfu/mL and 10 µL of each species were added to the wells. The plates were then incubated at optimum temperature for biofilm production and broth media was added in the wells aseptically if required. After the biofilm was developed, test compounds were added to the wells containing biofilm and incubated for 24 h at 37 °C for *M. smegmatis* and *M. fortuitum* and at 30 °C for *M. marinum*. The wells with biofilm but without test compounds were used as the control. The non-adherent cells were removed by washing the biofilms with PBS and were completely dried and desiccated. The samples treated with test compounds were observed under AFM (NTEGRA Prima) and the reduction of biofilm was determined with respect to control.

2.5.9. Colony forming assay

The anti-mycobacterial efficiency of PEG-AgNPs and AgNPs against *Mycobacterium* species was determined through colony counting assay. Overnight grown cultures of 0.5 McFarland were 1:100 diluted in broth medium and 100 µl diluted culture of each species were dispensed in 96-well flat bottom microtitre plate (Sigma-Aldrich) with PEG-AgNPs and AgNPs. The microtitre plates were sealed properly and incubated at respective temperatures i.e., *M. smegmatis* and *M. fortuitum* at 37 °C and *M. marinum* at 30 °C for 48 h. Afterward, 100 µl of treated cells of each species were plated on Middlebrook 7H10 agar plates and incubated for 3–4 days and colony-forming units (CFU) were observed.

3. Results and discussion

The rapid rise in drug-/multidrug-/extensively drug-resistant mycobacterial strains resistant to first-line drugs has made the quest for anti-TB agents an urgent clinical concern. A new paradigm in TB therapy that utilizes green-synthesized AgNPs may overcome these limitations. Historically, the anti-bacterial properties of medicinal plants have received the most attention from researchers. These plants are currently being investigated for new inhibitors that could counteract the resistance developed in mycobacterial species and help eliminate the threat posed by highly drug-resistant mycobacteria. Here, for the first time, we have reported the outstanding anti-mycobacterial and anti-biofilm potential of green-synthesized AgNPs using *C. serratum* extract encapsulated with polyethylene glycol polymer against the *Mycobacterium* species. Previous studies carried out on the synthesis of AgNPs using *C. serratum* extract demonstrated bactericidal effects on Gram-negative and Gram-positive bacteria [50] as well as anti-proliferative ability [31]; however, none of the studies have been reported that investigated the anti-mycobacterial activity of *C. serratum* extract alone or their green-synthesized AgNPs. Therefore, exploring the effects of green-synthesized AgNPs against mycobacteria is of great interest.

The present study describes an eco-friendly and economically viable method for synthesizing AgNPs using *C. serratum*. The concentration of the silver nitrate solution, the content of the PLE, time, temperature, and pH of the reaction mixture are only a few variables that affect the synthesis of AgNPs. The synthesis process was effective in terms of reaction time and stability of the synthesized nanoparticles, which do not contain external stabilizers or reducing agents. Thus, this reaction pathway satisfies every requirement for an entirely green chemical process.

3.1. Optimization for the preparation of AgNPs

The AgNPs from *C. serratum* leaves extract were synthesized as mentioned in sections 2.2-2.3. The change in color from yellow to brown indicated the formation of AgNPs (Figure S-1 in the ESM). Further, the prepared AgNPs were optimized based on critical factors such as sonication time, incubation time, and concentration of reducing agent (PLE), and further on, their particle size, and PDI were analyzed (Table 1). The optimization process of AgNP preparation leads to the development of AgNP-7 with a particle size of 31.68 nm

Table 1

Z-average size of optimized AgNPs by varying different conditions.

AgNPs	PLE/AgNO ₃ concentration ratio (mL)	Incubation time (hours)	Sonication time (minute)	Z-Average Particle size (nm)	PdI (Polydispersity Index)
1	5/45	–	–	440.2	0.595
2	5/45	–	5	248.2	0.200
3	5/45	–	10	73.03	0.250
4	2.5/47.5	–	10	121.9	0.271
5	4.5/45.5	–	10	90.58	0.284
6	6.5/43.5	–	10	91.36	0.301
7	5/45	1	10	31.68	0.288
8	5/45	2	10	133.7	0.223
9	5/45	6	10	152.2	0.242

showed the best formulation (Figure S-2 in the ESM).

Afterward, PEG-AgNPs were prepared with a Z-Average particle size of 49.78 nm with the best formulation AgNP-7 to control the nanoparticle physicochemical characteristics, surface aggregation shielding as well as a selective delivery to the affected site with lesser side effects.

3.2. Characterization of AgNPs

The synthesized AgNPs were characterized by several techniques such as UV-visible spectroscopy, Zetasizer, Zeta potential, High-performance liquid chromatography (HPLC), FTIR-ATR, X-ray diffraction (XRD), and HR-TEM.

3.2.1. Ultraviolet-visible spectroscopy

Ultraviolet-visible spectroscopy was used to determine the formation of metallic nanoparticles (AgNPs) by examining the optical characteristics, which are influenced by the size effect. The reduction of silver ions to nanoparticles was seen by monitoring the UV-Vis spectra of solutions. In the UV-visible spectrum a strong characteristic broad peak of AgNPs and PEG-encapsulated AgNPs were observed at 451 nm and 433 nm, respectively as shown in Fig. 1 (a). Hence, the wavelength and absorbance peaks were altered after the PEGylation of the AgNPs.

3.2.2. Charge analysis using zeta potential

The zeta potential of AgNPs and PEG-AgNPs was found to be +12.98 and +9.8 mV as shown in Fig. 1 (b). According to Abbas et al. 2015, AgNP's surface charge significantly affects their ability to kill both gram-positive and gram-negative bacteria. The positively charged NPs were found to be more potent as they disrupt cell walls due to the formation of strong bonds with membranes leading to enhancement in permeability [51]. Furthermore, a similar result was found by Aragão et al. in 2019 that higher positive Zeta potential leads to higher absorbance of AgNPs [52]. Since the Zeta potential of both AgNPs and PEG-AgNPs has higher positive values, they are

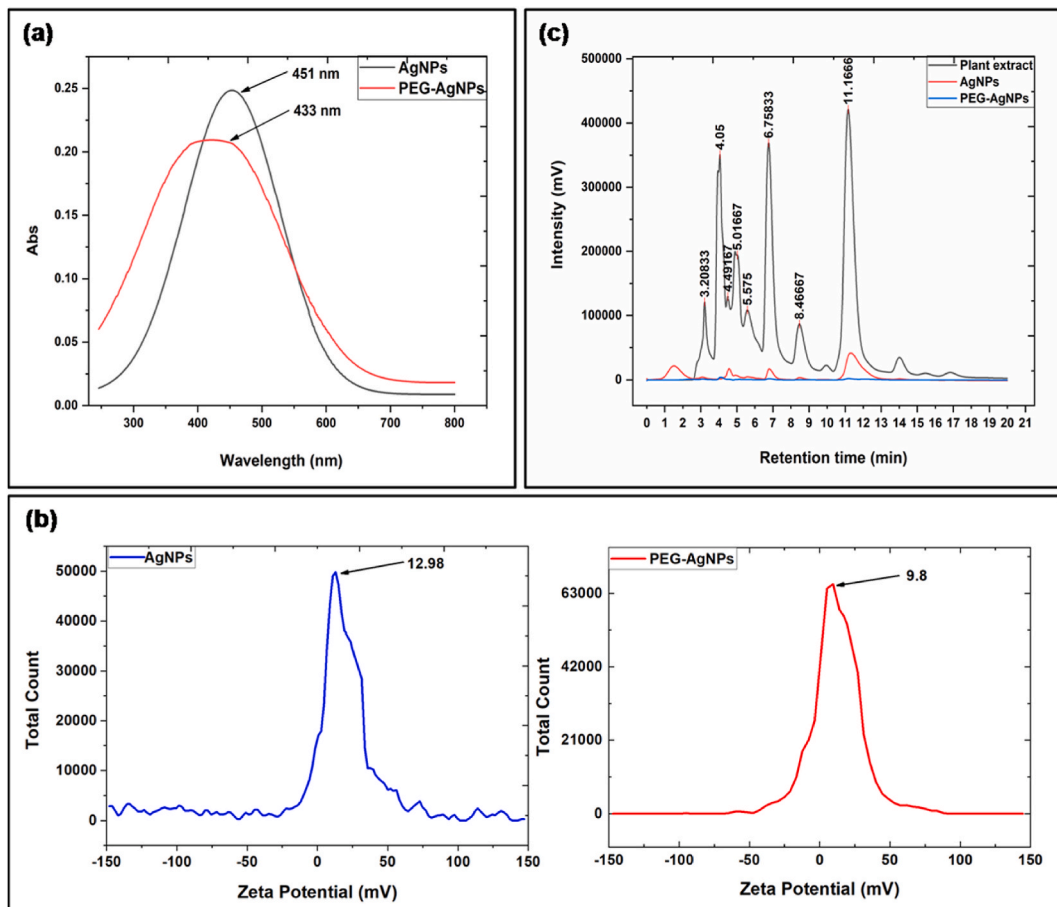


Fig. 1. (a) UV-Vis spectroscopy of nano-formulations (AgNPs and PEG-AgNPs). (b) Zeta potential of green-synthesized AgNPs and PEG-AgNPs. (c) HPLC data of Plant leaves extract (PLE), AgNPs, and PEG-AgNPs. (For interpretation of the references to color in this figure legend, the reader is referred to the Web version of this article.)

considered as stable in dispersed media with no agglomeration.

3.2.3. HPLC analysis

The plant *C. serratum* contains some phytoconstituents terpenoids (serratin, lupeol), flavonoids (catechin, hispidulin, cleroflavone, luteolin) and steroids (α -spinosteros, catechin, squalene), etc. [53], which play a significant role in reducing ions, leading to the synthesis of AgNPs. The chromatograms were drawn between intensity Vs retention time to identify the phytochemicals involved in the reduction of AgNO_3 in AgNPs. During isocratic conditions at room temperature, chromatograms of PLE, PEG, and PEG-AgNPs were obtained. The methanolic leaves extract chromatogram revealed the presence of principal phytochemicals luteolin, lupeol, catechin, and squalene with retention times 3.2 min, 4.49 min, 6.75 min, and 8.4 min, respectively as shown in Fig. 1 (c). The HPLC chromatographic spectra depict the presence of the phytoconstituent luteolin, a flavonoid that majorly participated in reducing AgNO_3 to AgNPs.

3.2.4. FTIR-ATR spectra

The FTIR-ATR spectral measurements were carried out to identify the potential biomolecules in *C. serratum* leaves extract which is responsible for reducing and capping the bio-reduced AgNPs. The results of FTIR-ATR analysis are shown in Fig. 2 (a). The two strong absorptions at 1599.08 and 1269.57 cm^{-1} represent the NO_2 group of the AgNO_3 molecule. FTIR-ATR spectra of PLE show various peaks of different functional groups viz, the broad peak from 3509.70 to 2400.77 cm^{-1} represents OH stretching of COOH group (carboxylic acid), 3186.05 – 3080.23 cm^{-1} represent sp^2 C–H stretching which means PLE has alkene group (sp^2 carbon), peaks at 2951.88 – 2786.55 cm^{-1} represent sp^3 C–H stretching, peak at 1811.51 cm^{-1} represents the presence of C=O groups of anhydride or acid chloride, peak at 1719.27 cm^{-1} represents the presence of C=O of ketone or aldehyde, peak at 1588 cm^{-1} represents C=C (alkene), and peak at 1034.32 cm^{-1} represent C–O group present in the PLE.

FTIR-ATR spectra of AgNPs show broad peaks at 3341 cm^{-1} due to the interaction of the OH group of alcohol or phenol with AgNPs, and a peak at 2917 , 1594 and 1040 cm^{-1} are due to the sp^3 C–H stretching, C=C of alkene group, CH_2 bending and C–O group of alcohol or ether, respectively. Along with these, FTIR spectra of PEG show peaks at 2859 , and 1456 cm^{-1} that correspond to the sp^3 C–H stretching, and CH_2 bending, and peaks at 1353 and 1051 cm^{-1} of C–O–C of PEG polymer, respectively. Further, the FTIR spectra of PEG-AgNPs show peaks at 3465 and 2893 cm^{-1} that correspond to the OH group of PEG polymer and sp^3 C–H stretching, respectively. In addition to this, other peaks at 1606 , 1344 , and 1150 cm^{-1} are due to the CH_2 bending and C–O–C of PEG polymer, respectively. The analysis of these spectra gives the conclusion that some functional groups of phytoconstituents present in plant extracts like ether, alcohol, and phenol interact with AgNO_3 to form AgNPs and adsorption of phenol, flavanones, and tannins type molecules on the metal surface of silver nanoparticles. Furthermore, it was concluded that the compatibility of compounds based on

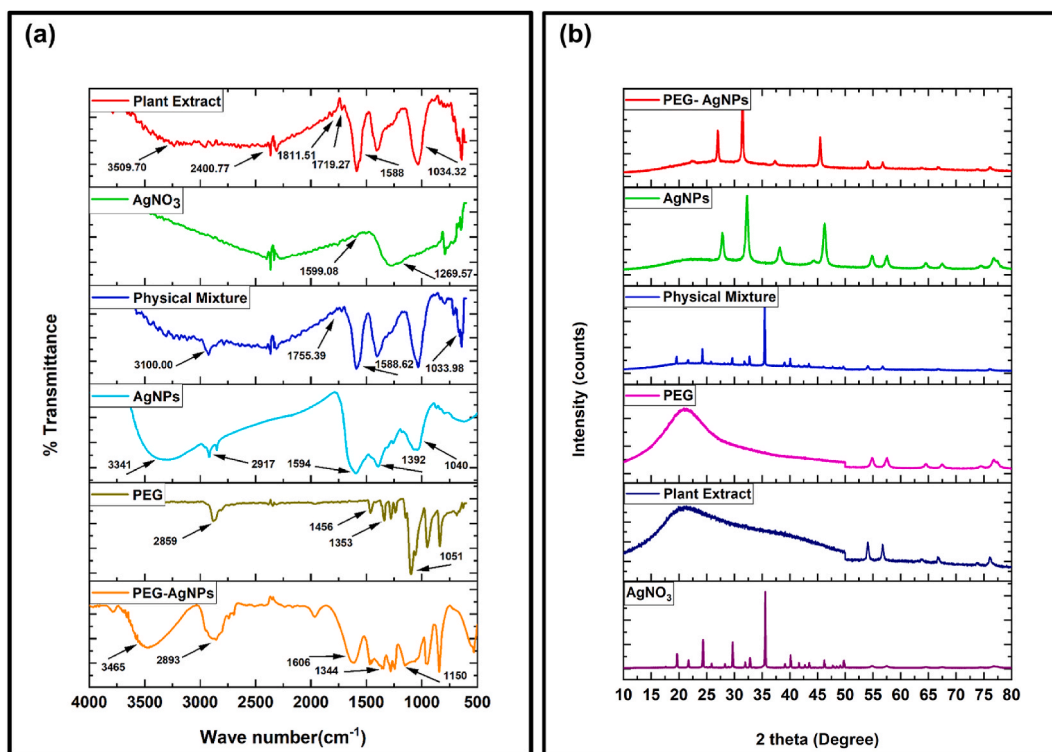


Fig. 2. (a) ATR spectra of Plant leaves extract (PLE), AgNO_3 , physical mixture, AgNPs, PEG, and PEG-AgNPs. (b) XRD data of PEG-AgNPs, AgNPs, physical mixture, PEG, Plant leaves extract, and AgNO_3 .

FTIR-ATR spectra of physical mixture shows no interference with the stretching and bending of compounds [54].

3.2.5. Crystallographic analysis

X-ray diffraction (XRD) is a widely used analytical method for observing the nature of crystalline metallic nanoparticles by penetrating the material with X-rays. Major peaks of AgNO_3 were observed at 2θ of 19.7° , 24.38° , 29.7° , 34.54° , and 40.14° , same are also present in the physical mixture as shown in Fig. 2 (b). In the case of the AgNPs and PEG-AgNPs, both show similar peaks at 2θ values of 27.86° , 32.24° and 46.18° . However, peaks of AgNPs at 38.21° , 54.72° , and 57.4° are diminished in the PEG-AgNPs, and peaks of AgNPs at 64.7° and 67.58° were absent in the PEG-AgNPs. The XRD of AgNO_3 shows its purity by exhibiting several sharp intense crystalline peaks at $2\theta = 26.94^\circ$, 32.34° and 46.34° .

3.2.6. Particle size measurement using Zetasizer and HR-TEM

The particle size of AgNPs and PEG-AgNPs was measured using the Zetasizer. Fig. 3 (a) depicts the Z-average particle size of AgNP and PEG-AgNP is 31.6 nm and 49.78 nm with PDI of 0.288 and 0.141, respectively. The lower PDI values of PEG-coated AgNPs inferred a more uniform size distribution than AgNPs.

Further, the shape, constitutive structure, and morphology of the nano-formulations were analyzed by transmission electron microscopy (HR-TEM). Fig. 3 (b) depicts the TEM image of AgNPs and PEG-AgNPs with a 100 nm scaling, at 10/1 electron diffraction, respectively. In the images with a 100 nm scale, the individual particles can be interpreted to be primarily spherical consist a particle size range of 9–35 nm for AgNPs and a particle size range of 15–60 nm for PEG-AgNPs [55]. The observation from HR-TEM shows the comparatively larger size distribution of the PEG-AgNPs as compared to AgNPs.

3.3. Biological evaluation of AgNPs

3.3.1. Anti-mycobacterial activity

The primary screening of synthesized PEG-AgNPs and AgNPs' anti-mycobacterial activity was carried out against *M. smegmatis*, *M. fortuitum*, and *M. marinum*. Linezolid was used as a positive control. The formation of a clear zone of inhibition in disk diffusion assay established the anti-mycobacterial efficacy of PEG-AgNPs and AgNPs against all three *Mycobacterium* species. In contrast, a very minimal visible zone was observed around the PLE disk, indicating it also has anti-mycobacterial potency. The diameter of the inhibition zone for PEG-AgNPs was higher than AgNPs and PLE against all three *Mycobacterium* species as shown in Fig. 4 (a) and Table 2.

To ascertain the anti-mycobacterial activity of green-synthesized AgNPs, MIC values were further determined. The MIC values of PEG-AgNPs, AgNPs, and PLE against *M. smegmatis*, *M. fortuitum*, and *M. marinum* have been shown in Table 2. The *Mycobacterium* species were found to be most susceptible to PEG-AgNPs followed by AgNPs. The MIC value of PEG-AgNPs was $0.39 \mu\text{g/mL}$ for *M. marinum* and $0.781 \mu\text{g/mL}$ for both *M. smegmatis* and *M. fortuitum*. Similarly, the MIC value of AgNPs was $0.781 \mu\text{g/mL}$ against *M. marinum* and $1.562 \mu\text{g/mL}$ against both *M. smegmatis* and *M. fortuitum*. All three species of *Mycobacterium* were less susceptible to PLE with a MIC value of 31.25 mg/mL . This may be due to various reasons *i.e.*, the large particle size of the extract unable to enter the cell wall of *Mycobacterium* cells, limited spectrum of activity, and lower potency. The concentration of active compounds in plant extract is generally lower when compared to reduced AgNPs and PEG-AgNPs which may not be sufficient to inhibit the growth of mycobacteria effectively, due to the presence of a thick outer cell wall.

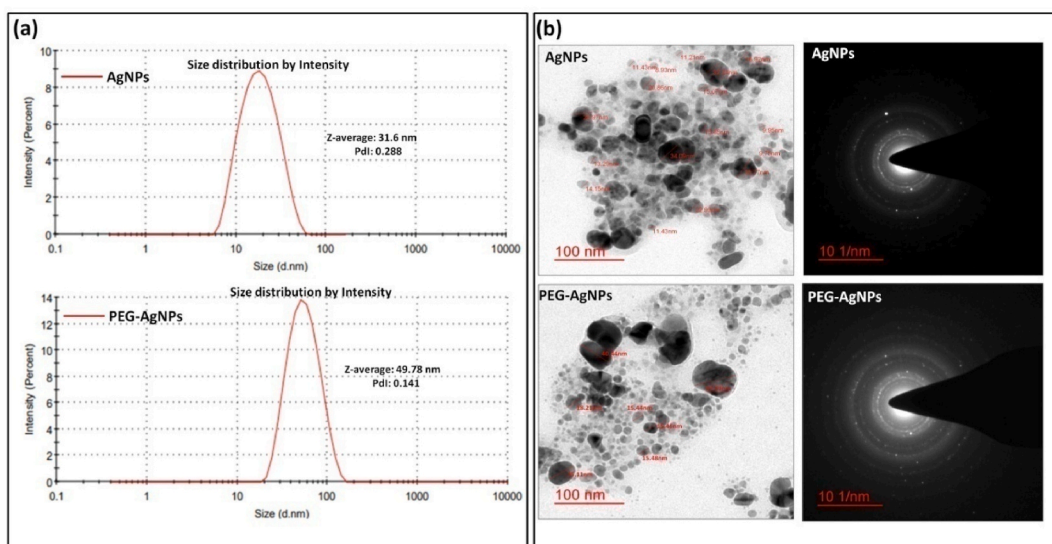


Fig. 3. (a) Z-average particle size of AgNPs and PEG-AgNPs. (b) TEM images of AgNPs and PEG-AgNPs with a 100 nm scaling, at 10/1 electron diffraction.

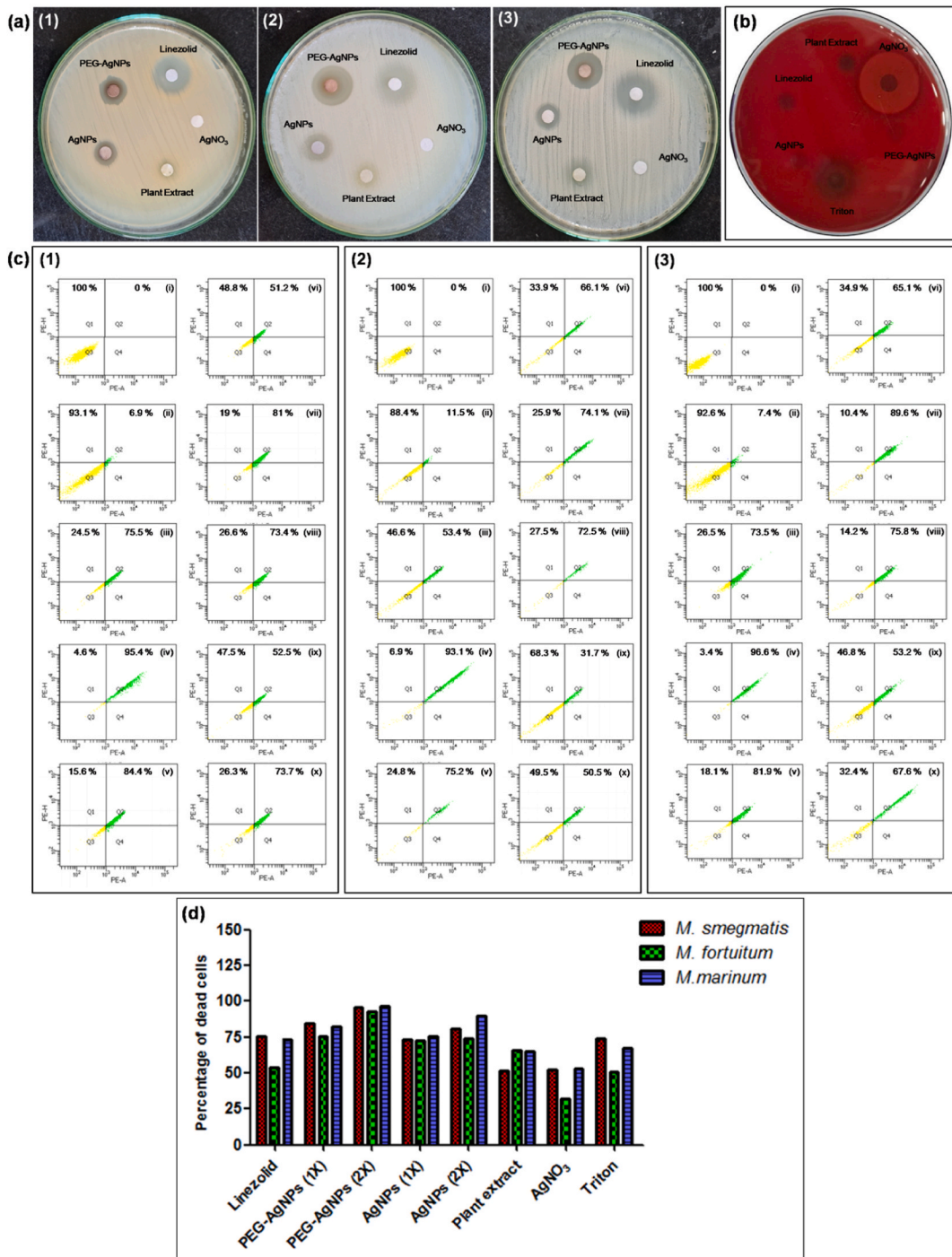


Fig. 4. (a) The figure shows the zone of inhibition of PEG-AgNPs, AgNPs, PLE, and AgNO₃ with Linezolid taken as a standard drug against the three *Mycobacterium* species i.e., (1) *M. smegmatis* (2) *M. fortuitum*, and (3) *M. marinum*. (b) Hemolytic activity of PEG-AgNPs (100 µg/mL), AgNPs (100 µg/mL), PLE (500 mg/mL), Linezolid (100 µg/mL), AgNO₃ (1 mM), and Triton X-100 (0.5 % v/v) on human blood agar. Triton X-100 and Linezolid were taken as positive control. (c) Flow cytometric analysis to determine the membrane damage of (1) *M. smegmatis* (2) *M. fortuitum*, and (3) *M. marinum*. (i–x) PI staining of all three *Mycobacterium* species (i) control without PI treatment, (ii) control with PI treatment, (iii) Linezolid, (iv) PEG-AgNPs (1X), (v) PEG-AgNPs (2X), (vi) Plant leaves extract, (vii) AgNPs (1X), (viii) AgNPs (2X), (ix) AgNO₃, and (x) Triton X-100. Linezolid and Triton X-100 were taken as positive controls. In each quadrant, Q₁ and Q₃ depict the percentage of live cells whereas Q₂ and Q₄ depict the percentage of dead cells. (d) Bar diagram representing the percentage of dead cells of *Mycobacterium* species treated with test compounds.

Table 2
Zone of inhibition and the MIC values of PEG-AgNPs, AgNPs, and PLE against *Mycobacterium* species.

Test compounds	Zone of inhibition (mm)			Minimum inhibitory concentration ($\mu\text{g/mL}$)		
	<i>M. smegmatis</i>	<i>M. fortuitum</i>	<i>M. marinum</i>	<i>M. smegmatis</i>	<i>M. fortuitum</i>	<i>M. marinum</i>
PEG-AgNPs	15 \pm 2	24 \pm 2	23 \pm 2	0.781	0.781	0.390
AgNPs	12 \pm 2	15 \pm 2	13 \pm 2	1.562	1.562	0.781
PLE	8 \pm 1	8 \pm 1	10 \pm 2	31250	31250	31250
AgNO ₃	–	–	–	–	–	–
Linezolid	20 \pm 2	23 \pm 2	24 \pm 2	2	4	1

#Antimycobacterial potency of PEG-AgNPs (100 $\mu\text{g/mL}$), AgNPs (100 $\mu\text{g/mL}$), Plant leaves extract (PLE) (500 mg/mL), and AgNO₃ (1 mM) compared with Linezolid (100 $\mu\text{g/mL}$) taken as positive control. The experiment was performed in triplicates ($n = 3$) and expressed as mean \pm standard deviation. The differences were significant as per the Mann-Whitney test ($p < 0.05$).

The observed MICs of the nanoparticles were also substantiated by earlier reports showing excellent anti-mycobacterial activity [56,57]. However, several *in vitro* studies suggest that Linezolid exhibits decisive anti-mycobacterial action against many resistant species of *Mycobacterium*, including Mtb. The MIC for Linezolid against XDR-TB clinical isolates of Mtb ranged from 0.125 $\mu\text{g/mL}$ to >2 $\mu\text{g/mL}$ [58]. The MICs of Linezolid for Mtb are lower than the MICs against other non-tuberculous mycobacteria (NTM). *M. smegmatis* and *M. fortuitum* are fast-growing NTM reported to have MIC values of 2 $\mu\text{g/mL}$ and 32 $\mu\text{g/mL}$ against Linezolid, respectively [59]. Braback et al. reported the MIC of Linezolid against *M. marinum* strains in the range of 0.5–4 ($\mu\text{g/mL}$) [60]. In our

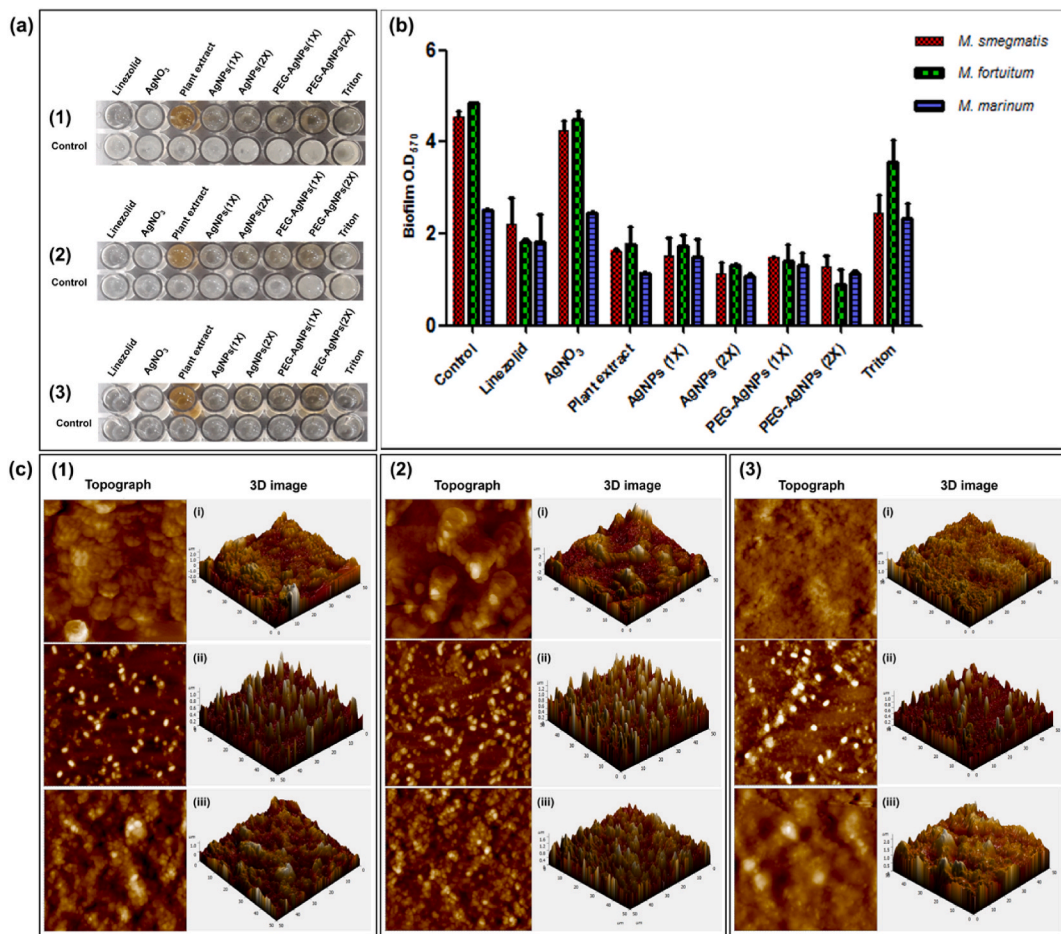


Fig. 5. (a) Biofilm inhibiting potential of PEG-AgNPs, AgNPs, and PLE was evaluated against (1) *M. smegmatis* (2) *M. fortuitum*, and (3) *M. marinum* using microtitre plate method. Triton X-100 and Linezolid were taken as positive control. (b) Crystal violet assay for quantification of biofilm inhibition using a spectrophotometer at 570 nm. The error bars on the graph represent the standard deviation from the mean ($n = 3$) of biofilm inhibition. (c) AFM images of biofilm surface of (1) *M. smegmatis* (2) *M. fortuitum* and (3) *M. marinum* taken at the $50 \times 50 \mu\text{m}$ scan in the tapping mode. (i) Control without treatment (ii) PEG-AgNPs (iii) AgNPs. (For interpretation of the references to color in this figure legend, the reader is referred to the Web version of this article.)

study, the AgNPs synthesized from *C. serratum* leaves extract and its PEGylated form were tested against *M. smegmatis*, *M. fortuitum*, and *M. marinum* and MIC values obtained were comparably less than the MICs mentioned for NTM species. The MIC values for PEG-AgNPs against *M. smegmatis*, *M. fortuitum*, and *M. marinum* were 0.781 $\mu\text{g/mL}$, 0.781 $\mu\text{g/mL}$, and 0.39 $\mu\text{g/mL}$, respectively which indicate PEG-AgNPs synthesized from *C. serratum* extract is a promising alternative to Linezolid.

In corroboration, the culture of all three *Mycobacterium* species was treated with PEG-AgNPs and AgNPs at 2X concentration, i.e., twice the concentration initially taken for the MIC determination, and plated on Middlebrook 7H10 agar plates to evaluate their viability. After incubation for 3–4 days, there was a significant reduction in colony-forming units of all three species treated with PEG-AgNPs and AgNPs as shown in Figure S-3 in the ESM. This further confirms the anti-mycobacterial efficiency of PEG-AgNPs and AgNPs.

3.3.2. Hemolytic activity

The hemolytic activity of PEG-AgNPs, AgNPs, PLE, and AgNO_3 was evaluated on the human blood agar plate. After incubation for 24 h, a hemolytic zone of inhibition was observed around the disk loaded with AgNO_3 and Triton whereas no visible zone was present around PEG-AgNPs, AgNPs, PLE as shown in Fig. 4 (b). The formation of a clear visible zone indicates the potential to induce hemolysis. This implies that PEG-AgNPs, AgNPs, and PLE have no toxic effect on human RBCs.

3.3.3. Analysis of membrane damage using flow cytometry

The membrane-induced damage due to the treatment with test compounds leads to the lysis of mycobacterial cells. The permeabilization of the cytoplasmic membrane consequently results in the loss of nuclear DNA content, evaluated through propidium iodide (PI) flow cytometric assay. The PI used in the analysis, binds to the DNA and quantifies the dead cells [48]. Two different concentrations (1X and 2X) of AgNPs and PEG-AgNPs were taken to quantify the lysis. The percentage of dead cells after exposure to 1X PEG-AgNPs were 84.4 %, 75.2 %, and 81.9 % while the percentage of dead cells after exposure to 1X AgNPs were 73.4 %, 72.5 %, and 75.8 % for *M. smegmatis*, *M. fortuitum* and *M. marinum*, respectively. Similarly, the percentage of dead cells after exposure to 2X PEG-AgNPs was 95.4 %, 93.1 %, and 96.6 % while the percentage of dead cells after exposure to 2X AgNPs were 81 %, 74.1 %, and 89.6 % for *M. smegmatis*, *M. fortuitum* and *M. marinum*, respectively. The result showed that PEG-AgNPs induced more damage to all three *Mycobacterium* species as compared to AgNPs and PLE as shown in Fig. 4 (c) and (d). The flow cytometry results further suggest that the lysis induced by a 1X concentration of NPs is comparatively higher than the Linezolid, whereas the 2X concentration of PEG-AgNPs leads to almost complete lysis of all three *Mycobacterium* species. The induced damages to the membrane organization upon treatment with PEG-AgNPs were highest in *M. marinum* as compared to *M. smegmatis* and *M. fortuitum*. The resultant lysis pattern of NPs against mycobacterium species suggests that the green-synthesized AgNPs from *C. serratum* are probably more potent to Linezolid and they may have different modes of action. Further, AgNPs coated with polyethylene glycol have improved efficiency against the mycobacterial target cells.

3.3.4. Biofilm inhibition propensity

The formation of biofilm by *Mycobacterium* species during infection is manifested by protection against the antibiotics that are normally efficient against the same bacteria in their planktonic forms. This leads to the development of antimicrobial resistance and finally treatment failure. Therefore, the biofilm inhibitory activity of AgNPs and PEG-AgNPs was evaluated further. At first, the biofilm-forming potential of *Mycobacterium* species was analyzed using the microtitre plate method. Figure S-4 in the ESM showed that all three *Mycobacterium* species have a biofilm-forming ability which was quantified using the crystal violet method. *M. fortuitum* exhibited the highest level of biofilm formation among the three whereas, *M. marinum* showed minimum biofilm-forming potential incubated at 30 °C for 4 days as compared to *M. smegmatis*, and *M. fortuitum* incubated at 37 °C for 4 days.

Further, the biofilm inhibition propensity of PEG-AgNPs, AgNPs, and PLE were evaluated. The results showed that the biofilm of *Mycobacterium* species was significantly inhibited by PEG-AgNPs and AgNPs *in vitro* as shown in Fig. 5 (a) and (b). The biofilm treated with 1X concentration of PEG-AgNPs and AgNPs exhibited greater reduction with respect to the positive control (Linezolid and Triton X-100) and PEG-AgNPs being most effective. Surprisingly, biofilm treated with PLE also showed a significant reduction in biofilm but not as efficient as compared to the PEG-AgNPs and AgNPs. The anti-biofilm activity of PLE against mycobacterial species indicates the presence of bioactive compounds in the extract that may not have the greater efficacy to reach the target inside the cell but have considerable potency to degrade the extracellular polymeric substances of the biofilm layer.

Table 3

Topographic statistics of biofilm surfaces analyzed through AFM.

<i>Mycobacterium</i> species	Sample	Height (max)	Roughness average (R_a)	Root mean square (RMS)	Skewness (Ssk)	Kurtosis (Ska)
1. <i>M. smegmatis</i>	A. Control	2.512 μm	0.441 μm	0.570 μm	0.196	4.193
	B. PEG-AgNPs treated	700.909 nm	108.964 nm	154.123 nm	1.428	5.778
	C. AgNPs treated	1.636 μm	0.359 μm	0.464 μm	0.265	3.492
2. <i>M. fortuitum</i>	A. Control	4.293 μm	1.067 μm	1.340 μm	0.0621	2.756
	B. PEG-AgNPs treated	738.543 nm	138.287 nm	177.590 nm	0.921	3.604
	C. AgNPs treated	984.09 nm	185.291 nm	233.277 nm	0.287	3.102
3. <i>M. marinum</i>	A. Control	1.307 μm	0.190 μm	0.248 μm	-0.369	4.396
	B. PEG-AgNPs treated	806.708 nm	111.632 nm	152.931 nm	1.898	6.971
	C. AgNPs treated	1.058 μm	0.176 μm	0.233 μm	-0.0164	4.207

3.3.5. Analysis of biofilm disruption using AFM

The disruption of biofilm produced by *M. smegmatis*, *M. fortuitum*, and *M. marinum* after treatment with PEG-AgNPs and AgNPs was analyzed using AFM. The characteristics of the surface investigated to evaluate biofilm disruption were height (maximum), root mean square (RMS), roughness average (R_a), skewness (Ssk), and kurtosis (Ska) and their difference with respect to control. The root mean square is the standard deviation of the height distribution with respect to the mean plane on the surface [61]. Skewness and kurtosis both are dimensionless quantities. While skewness measures the asymmetry of the distribution, kurtosis measures the sharpness of the peak in the distribution. When the skewness value is negative, the surface is dominated by “holes” or “valleys”, while a positive value shows that the surface is dominated by “hills” [49]. The topography of the biofilm treated with 2X PEG-AgNPs and AgNPs showed a significant decrease in the height and roughness with respect to control in all three *Mycobacterium* species as shown in Fig. 5 (c) and Table 3. The result demonstrated that the biofilm treated with PEG-AgNPs showed decreased adherence of cells onto the surface as compared to the control.

The height of biofilm produced by *M. smegmatis* upon treatment with PEG-AgNPs and AgNPs was found to be 700.909 nm and 1.636 μm , respectively with respect to the control with a height of 2.512 μm . On the other hand, roughness decreased to 108.964 nm (PEG-AgNPs treated) and 0.359 μm (AgNPs treated) from 0.441 μm (control).

The height profile of *M. fortuitum* biofilm revealed a significant decrease from 4.293 μm (control) to 738.543 nm and 984.09 nm, and also a decrease in roughness from 1.067 μm (control) to 138.287 nm and 185.291 nm after treatment with PEG-AgNPs and AgNPs, respectively. Similarly for *M. marinum*, the height of biofilm upon treatment with PEG-AgNPs and AgNPs was found to be 806.708 nm and 1.058 μm , respectively while that of control was 1.307 μm . The roughness of control decreased from 0.190 μm (control) to 111.632 nm and 0.176 μm after treatment with PEG-AgNPs and AgNPs, respectively. The negative skewness values of control and AgNPs treated *M. marinum* biofilms indicated that the surface was dominated by “holes” or “valleys”.

Therefore, the results elucidate that both PEG-AgNPs and AgNPs exhibit anti-biofilm propensity; however, PEG-AgNPs had more significant biofilm-degrading potential than AgNPs and Linezolid. A recent work done by Oziri et al. established that PEGylation of AgNPs drastically enhanced its dispersion stability and exhibited persistent antimicrobial activity [62]. In addition, the AFM image depicts the PEG-AgNP-treated biofilm of all three species of *Mycobacterium* species, showing a remarkable reduction in the thickness and height of the biofilm, establishing its promising therapeutic ability in the treatment of TB.

In summary, we demonstrated that the anti-mycobacterial activity of the synthesized nanoparticles was better than that of Linezolid, both in its planktonic and biofilm states. Linezolid is an oxazolidinone that binds to the P site on the ribosomal 50S subunit to prevent protein synthesis; however, multiple mechanisms of anti-bacterial activity of green-synthesized AgNPs have been deciphered to date, such as adherence to the bacterial cell wall because of the electrostatic interaction and subsequent destabilization of the cell leading to the lysis and generation of free radicals that are reactive oxygen species (ROS), inhibition of several cellular metabolic processes, inhibition of bacterial DNA replication, alteration of gene expression, alteration of ATP synthesis, and disruption of the microorganism's respiratory chain at the level of cytochrome oxidase. AgNPs can exert multi-target effects on biofilms, making them effective against various stages of biofilm formation and maintenance. They can disrupt the biofilm matrix, destabilize bacterial cell membranes, inhibit cellular respiration, and induce oxidative stress [63]. These multiple modes of action make AgNPs probably more effective in targeting and eradicating biofilms than antibiotics with single-target mechanisms, such as linezolid. While the study provides promising findings regarding the anti-mycobacterial activity of AgNPs and PEG-AgNPs, it is important to acknowledge the potential limitations of the study. The study primarily focuses on *in vitro* evaluations of AgNPs and PEG-AgNPs against three *Mycobacterium* species. However, *in vitro* assays may not fully represent the complexities of *in vivo* conditions, such as host immune responses and pharmacokinetics, which are crucial for assessing the therapeutic potential of these nanoparticles. Further investigations are needed to elucidate their mechanism of action and efficacy in animal models of TB infection. *In vivo* studies would provide valuable insights into the bio-distribution, tissue penetration, and potential adverse effects of these nanoparticles. Current study demonstrates the absence of hemolytic activity against human RBCs, however comprehensive toxicity assessments, including cytotoxicity studies on relevant cell lines and evaluation of potential immunogenicity and organ toxicity in animal models, are necessary to establish the safety profile of PEG-AgNPs for therapeutic use. Further research with clinical mycobacterial strains, including MDR strains, would enhance the applicability of the findings.

Despite its limitations, this work is valuable for TB research due to its promising insights into the potential of green-synthesized AgNPs and their derivatives against biofilm-forming mycobacterial strains. Thorough characterization of the nanoparticles and demonstration of their anti-mycobacterial activity provides a strong foundation for further research. Additionally, its emphasis on safety highlights their potential as safer alternatives to existing therapies, contributing valuable knowledge to the field.

4. Conclusion

This is the first study to report the efficient and environment friendly synthesis of AgNPs using *C. serratum* aqueous leaves extract and to establish their efficacy against *Mycobacterium* species. *M. smegmatis* is used as a surrogate for Mtb due to its genetic similarity, fast growing ability and non-pathogenic nature while *M. marinum*, a close relative of Mtb causes fish tank granuloma, and occasionally affects humans have also been studied. The study showed that green-synthesized AgNPs have excellent anti-mycobacterial activity against *M. smegmatis*, *M. fortuitum*, and *M. marinum*. By examining how these mycobacterial species respond to green-synthesized AgNPs and PEG-AgNPs, this study not only confirmed their potential as anti-mycobacterial agents against TB but also offered comprehensive insights into combating other mycobacterial infections caused by both Tubercular and NTM. The association between these strains and the Mtb amplifies the significance of our findings, potentially benefiting clinical applications in TB therapy. It was further established that both the anti-mycobacterial and anti-biofilm abilities of AgNPs increased upon encapsulation with PEG. These

findings imply that the increased bioavailability of green-synthesized AgNPs is an additional advantage of PEG encapsulation, which may offer a novel therapeutic approach to address the limitations of existing TB therapies, thus making it a promising therapeutic alternative. Our research can contribute to providing a new pathway for the development of nanomedicines by employing green synthesis. However, a comprehensive study is required to fully understand the mechanism of action of AgNPs in anticipation of their broader and meaningful roles in the medical fraternity. Nevertheless, *in vivo* research is necessary to address the challenges associated with the application of green-synthesized nanomaterials, such as their pharmacokinetic and pharmacodynamic properties.

Ethics declarations

Review or approval by an ethics committee was not needed for this study because this work does not involve animal experiments or human samples.

Funding statement

This work was supported by the University Grant Commission (UGC), (M-14/84), Start-up grant, New Delhi, and Institute of Eminence grant, Scheme no. 6031, BHU, Varanasi, India. In addition, VS is grateful to the CSIR, New Delhi for providing the JRF-NET Fellowship. RRP and SKS want to thank Banaras Hindu University (BHU), Varanasi, India for providing the UGC Non-NET Fellowship and Malaviya Postdoctoral Fellowship (MPDF), respectively.

Data availability statement

The corresponding author will provide the datasets used and analyzed in the study upon reasonable request.

CRedit authorship contribution statement

Vidyasagar: Writing – original draft, Visualization, Validation, Software, Methodology, Investigation, Formal analysis, Data curation. **Ritu Raj Patel:** Writing – original draft, Visualization, Validation, Software, Methodology, Investigation, Formal analysis, Data curation. **Sudhir Kumar Singh:** Writing – review & editing, Writing – original draft, Visualization, Validation, Software, Methodology, Investigation, Formal analysis, Data curation. **Deepa Dehari:** Investigation, Formal analysis, Data curation. **Gopal Nath:** Writing – review & editing. **Meenakshi Singh:** Writing – review & editing, Validation, Supervision, Methodology, Funding acquisition, Conceptualization.

Declaration of competing interest

The authors declare that they have no known competing financial interests or personal relationships that could have appeared to influence the work reported in this paper.

Acknowledgments

We would like to thank CDC-BHU, ISLS-BHU, and IIT-BHU for providing the technical, instrumental, and biological activities support.

Appendix A. Supplementary data

Supplementary data to this article can be found online at <https://doi.org/10.1016/j.heliyon.2024.e31116>.

Electronic supplementary material

Supplementary material (change in color during synthesis of AgNPs using plant leaves extract, Z-average particle size of samples, colony forming assay of *M. smegmatis*, *M. fortuitum* and *M. marinum* treated with 2X MICs of PEG-AgNPs and AgNPs using spread plate technique, and biofilm forming potential of *M. smegmatis*, *M. fortuitum* and *M. marinum* under *in vitro* conditions) is available in the online version of this article at.

References

- [1] C.J. Meehan, R.A. Barco, Y.H.E. Loh, S. Cogneau, L. Rigouts, Reconstituting the genus *Mycobacterium*, *Int. J. Syst. Evol. Microbiol.* 71 (2021) 004922.
- [2] M.A. Forrellad, L.I. Klepp, A. Gioffré, J. Sabio y Garcia, H.R. Morbidoni, M.D.L.P. Santangelo, A.A. Cataldi, F. Bigi, Virulence factors of the *Mycobacterium tuberculosis* complex, *Virulence* 4 (2013) 3–66.

- [3] K. Thangavelu, K. Krishnakumariam, G. Pallam, D.D. Prakash, L. Chandrashekar, E. Kalaiarasan, S. Das, M. Muthuraj, N.M. Joseph, Prevalence and speciation of non-tuberculous mycobacteria among pulmonary and extrapulmonary tuberculosis suspects in South India, *Journal of Infection and Public Health* 14 (2021) 320–323.
- [4] Y. Shen, X. Wang, J. Jin, J. Wu, X. Zhang, J. Chen, W. Zhang, In vitro susceptibility of *Mycobacterium abscessus* and *Mycobacterium fortuitum* isolates to 30 antibiotics, *BioMed Res. Int.* 2018 (2018) 1–10.
- [5] E. Hashish, A. Merwad, S. Elgaml, A. Amer, H. Kamal, A. Elsayed, A. Marei, M. Sitohy, *Mycobacterium marinum* infection in fish and man: epidemiology, pathophysiology and management; a review, *Vet. Q.* 38 (2018) 35–46.
- [6] <https://www.who.int/teams/global-tuberculosis-programme/tb-reports/global-tuberculosis-report-2022>. (Accessed 17 January 2023).
- [7] R.B. Patel, B.B. Patel, An analysis of the COVID-19 situation in India in terms of testing, treatment, vaccine acceptance and national economic performance, *Int. J. Publ. Health* 67 (2022) 249.
- [8] D.R. Silva, M. Dalcolmo, S. Tiberi, M.A. Arbex, M. Munoz-Torrico, R. Duarte, L. D'Ambrosio, D. Visca, A. Rendon, M. Gaga, A. Zumla, New and repurposed drugs to treat multidrug- and extensively drug-resistant tuberculosis, *J. Bras. Pneumol.* 44 (2018) 153–160.
- [9] J. Esteban, M. Garcia-Coca, *Mycobacterium* biofilms, *Front. Microbiol.* 8 (2018) 2651.
- [10] S. Ilic, S. Cohen, M. Singh, B. Tam, A. Dayan, B. Akabayov, DnaG primase—a target for the development of novel antibacterial agents, *Antibiotics* 7 (2018) 72.
- [11] N.G. Bajad, S.K. Singh, S.K. Singh, T.D. Singh, M. Singh, Indole: a promising scaffold for the discovery and development of potential anti-tubercular agents, *Current Research in Pharmacology and Drug Discovery* 3 (2022) 100119.
- [12] S. Sellamuthu, M. Singh, A. Kumar, S.K. Singh, Type-II NADH Dehydrogenase (NDH-2): a promising therapeutic target for antitubercular and antibacterial drug discovery, *Expert Opin. Ther. Targets* 21 (2017) 559–570.
- [13] V. Sagar, R.R. Patel, S.K. Singh, M. Singh, Green synthesis of silver nanoparticles: methods, biological applications, delivery and toxicity, *Materials Advances* 4 (2023) 1831–1849.
- [14] R. Kumar, G. Ghoshal, A. Jain, M. Goyal, Rapid green synthesis of silver nanoparticles (AgNPs) using (*Prunus persica*) plants extract: exploring its antimicrobial and catalytic activities, *J. Nanomed. Nanotechnol.* 8 (2017) 1–8.
- [15] V.K. Sharma, R.A. Yngard, Y. Lin, Silver nanoparticles: green synthesis and their antimicrobial activities, *Adv. Colloid Interface Sci.* 145 (2009) 83–96.
- [16] S. Jain, M.S. Mehata, Medicinal plant leaf extract and pure flavonoid mediated green synthesis of silver nanoparticles and their enhanced antibacterial property, *Sci. Rep.* 7 (2017) 15867.
- [17] J.K. Patra, G. Das, L.F. Fraceto, E.V.R. Campos, M.D.P. Rodriguez-Torres, L.S. Acosta-Torres, L.A. Diaz-Torres, R. Grillo, M.K. Swamy, S. Sharma, S. Habtemariam, H.S. Shin, Nano based drug delivery systems: recent developments and future prospects, *J. Nanobiotechnol.* 16 (2018) 1–33.
- [18] A.C. Burduşel, O. Gherasim, A.M. Grumezescu, L. Mogoantă, A. Ficiu, E. Andronescu, Biomedical applications of silver nanoparticles: an up-to-date overview, *Nanomaterials* 8 (2018) 681.
- [19] K.J. Seung, S. Keshavjee, M.L. Rich, Multidrug-resistant tuberculosis and extensively drug-resistant tuberculosis, *Cold Spring Harbor perspectives in medicine* 5 (2015) a017863.
- [20] D. Kamarudin, N.A. Hashim, B.H. Ong, C.R. Che Hassan, N. Abdul Manaf, Synthesis of silver nanoparticles stabilised by pvp for polymeric membrane application: a comparative study, *Mater. Technol.* 37 (2022) 289–301.
- [21] A. Abdelfattah, A.E. Aboutaleb, A.B.M. Abdel-Aal, A.A. Abdellatif, H.M. Tawfeek, S.I. Abdel-Rahman, Design and optimization of PEGylated silver nanoparticles for efficient delivery of doxorubicin to cancer cells, *J. Drug Deliv. Sci. Technol.* 71 (2022) 103347.
- [22] A. Salayová, Z. Bedvičová, N. Daneu, M. Baláz, Z. LukáčováBujňáková, L. Balázová, L. Tkáčiková, Green synthesis of silver nanoparticles with antibacterial activity using various medicinal plant extracts: morphology and antibacterial efficacy, *Nanomaterials* 11 (2021) 1005.
- [23] S. Palkhiwala, S.R. Bakshi, Engineered nanoparticles: revisiting safety concerns in light of ethno medicine, *AYU Int. Q. J. Res. Ayurveda.* 35 (2014) 237.
- [24] P. Moteriya, S. Chanda, Synthesis and characterization of silver nanoparticles using *Caesalpinia pulcherrima* flower extract and assessment of their in vitro antimicrobial, antioxidant, cytotoxic, and genotoxic activities, *Artif. Cell Nanomed. Biotechnol.* 45 (2017) 1556–1567.
- [25] M. Oves, M.A. Rauf, M. Aslam, H.A. Qari, H. Sonbol, I. Ahmad, G.S. Zaman, M. Saeed, Green synthesis of silver nanoparticles by *ConocarpusLancifolius* plant extract and their antimicrobial and anticancer activities, *Saudi J. Biol. Sci.* 29 (2022) 460–471.
- [26] World Health Organization, The World Traditional Medicines Situation. *Traditional Medicines: Global Situation*, vol. 3, Issues and Challenges, Geneva, 2011, pp. 1–14.
- [27] V. De Luca, V. Salim, S.M. Atsumi, F. Yu, Mining the biodiversity of plants: a revolution in the making, *Science* 336 (2012) 1658–1661.
- [28] J.J. Patel, S.R. Acharya, N.S. Acharya, *Clerodendrum serratum* (L.) Moon.—A review on traditional uses, phytochemistry and pharmacological activities, *J. Ethnopharmacol.* 154 (2014) 268–285.
- [29] <https://pcimh.gov.in/WriteReadData/RTF1984/1536815619.pdf>. (Accessed 2 February 2023).
- [30] A.B. Patil, S.K. Mengane, Green synthesis of silver nano particles from *Clerodendrum serratum* and antimicrobial activity against human pathogens, *J. Bionanoscience* 10 (2016) 491–494.
- [31] R.P. Raman, S. Parthiban, B. Srinithya, V.V. Kumar, S.P. Anthony, A. Sivasubramanian, M.S. Muthuraman, Biogenic silver nanoparticles synthesis using the extract of the medicinal plant *Clerodendron serratum* and its in-vitro antiproliferative activity, *Mater. Lett.* 160 (2015) 400–403.
- [32] I.L. Sparks, K.M. Derbyshire, Jr W.R. Jacobs, Y.S. Morita, *Mycobacterium smegmatis*: the vanguard of mycobacterial research, *J. Bacteriol.* 205 (2023) e00337.
- [33] D.M. Tobin, L. Ramakrishnan, Comparative pathogenesis of *Mycobacterium marinum* and *Mycobacterium tuberculosis*, *Cell Microbiol.* 10 (2008) 1027–1039.
- [34] J.M. Ashraf, M.A. Ansari, H.M. Khan, M.A. Alzohairy, I. Choi, Green synthesis of silver nanoparticles and characterization of their inhibitory effects on AGEs formation using biophysical techniques, *Sci. Rep.* 6 (2016) 1–10.
- [35] D.M. Pawde, M.K. Viswanadh, A.K. Mehata, R. Sonkar, S. Poddar, A.S. Burande, A. Jha, K.Y. Vajanthri, S.K. Mahto, V.A. Dustakeer, M.S. Muthu, Mannose receptor targeted bioadhesive chitosan nanoparticles of clofazimine for effective therapy of tuberculosis, *Saudi Pharmaceut. J.* 28 (2020) 1616–1625.
- [36] M.A. Rather, I.A. Bhat, N. Sharma, A. Gora, P.A. Ganie, R. Sharma, Synthesis and characterization of *Azadirachta indica* constructed silver nanoparticles and their immunomodulatory activity in fish, *Aquacult. Res.* 48 (2017) 3742–3754.
- [37] C. Singh, J. Kumar, P. Kumar, B.S. Chauhan, K.N. Tiwari, S.K. Mishra, S. Srikrishna, R. Saini, G. Nath, J. Singh, Green synthesis of silver nanoparticles using aqueous leaf extract of *Premna integrifolia* (L.) rich in polyphenols and evaluation of their antioxidant, antibacterial and cytotoxic activity, *Biotechnol. Equip.* 33 (2019) 359–371.
- [38] M.A. Ansari, H.M. Khan, M.A. Alzohairy, M. Jalal, S.G. Ali, R. Pal, J. Musarrat, Green synthesis of Al₂O₃ nanoparticles and their bactericidal potential against clinical isolates of multi-drug resistant *Pseudomonas aeruginosa*, *World J. Microbiol. Biotechnol.* 31 (2015) 153–164.
- [39] S. Khodadadi, N. Mahdinezhad, B. Fazeli-Nasab, M.J. Heidari, B. Fakheri, A. Miri, Investigating the possibility of green synthesis of silver nanoparticles using *Vaccinium arctostaphylos* extract and evaluating its antibacterial properties, *BioMed Res. Int.* 2021 (2021) 1–13.
- [40] E.J. De Beer, M.B. Sherwood, The paper-disc agar-plate method for the assay of antibiotic substances, *J. Bacteriol.* 50 (1945) 459–467.
- [41] M. Singh, S.K. Singh, M. Gangwar, G. Nath, S.K. Singh, Design, synthesis and mode of action of novel 2-(4-aminophenyl) benzothiazole derivatives bearing semicarbazone and thiosemicarbazone moiety as potent antimicrobial agents, *Med. Chem. Res.* 25 (2016) 263–282.
- [42] G. O'Toole, H.B. Kaplan, R. Kolter, Biofilm formation as microbial development, *Annu. Rev. Microbiol.* 54 (2000) 49–79.
- [43] R.P. Dewangan, M. Singh, S. Ilic, B. Tam, B. Akabayov, Cell-penetrating peptide conjugates of indole-3-acetic acid-based DNA primase/Gyrase inhibitors as potent anti-tubercular agents against planktonic and biofilm culture of *Mycobacterium smegmatis*, *Chem. Biol. Drug Des.* 98 (2021) 722–732.
- [44] P. Chakraborty, S. Bajeli, D. Kaushal, B.D. Radotra, A. Kumar, Biofilm formation in the lung contributes to virulence and drug tolerance of *Mycobacterium tuberculosis*, *Nat. Commun.* 12 (2021) 1606.
- [45] <https://clsi.org/standards/products/microbiology/documents/m27/>. (Accessed 17 May 2022).
- [46] G.E. Rowe, R.A. Welch, [53] Assays of hemolytic toxins, *Methods Enzymol.* 235 (1994) 657–667.
- [47] C. Riccardi, I. Nicoletti, Analysis of apoptosis by propidium iodide staining and flow cytometry, *Nat. Protoc.* 1 (2006) 1458–1461.

- [48] M. Singh, S.K. Singh, M. Gangwar, G. Nath, S.K. Singh, Design, synthesis and mode of action of some benzothiazole derivatives bearing an amide moiety as antibacterial agents, *RSC Adv.* 4 (2014) 19013–19023.
- [49] S. Chatterjee, N. Biswas, A. Datta, R. Dey, P. Maiti, Atomic force microscopy in biofilm study, *Microscopy* 63 (2014) 269–278.
- [50] A.B. Patil, S.K. Mengane, Green synthesis of silver nano particles from *clerodendrumserratum* and antimicrobial activity against human pathogens, *J. Bionanoscience* 10 (2016) 491–494.
- [51] A. Abbaszadegan, Y. Ghahramani, A. Gholami, B. Hemmateenejad, S. Dorostkar, M. Nabavizadeh, H. Sharghi, The effect of charge at the surface of silver nanoparticles on antimicrobial activity against gram-positive and gram-negative bacteria: a preliminary study, *J. Nanomater.* 16 (2015) 53, 53.
- [52] A.P. de Aragao, T.M. de Oliveira, P.V. Quelemes, M.L.G. Perfeito, M.C. Araujo, J.D.A.S. Santiago, V.S. Cardoso, P. Quaresma, J.R.D.S. de Almeida, D.A. da Silva, Green synthesis of silver nanoparticles using the seaweed *Gracilariabirdiae* and their antibacterial activity, *Arab. J. Chem.* 12 (2019) 4182–4188.
- [53] P. Kumar, K. Nishteswar, Phytochemical and pharmacological profiles of *Clerodendrum serratum*linn.(bharngi): a review, *Int. J. Res. Ayurveda Pharm.* 4 (2013) 276–278.
- [54] A.S. Mohamad Kasim, A.B. Ariff, R. Mohamad, F.W.F. Wong, Interrelations of synthesis method, polyethylene glycol coating, physico-chemical characteristics, and antimicrobial activity of silver nanoparticles, *Nanomaterials* 10 (2020) 2475.
- [55] K.S. Desai, T.C. Taranath, Characterization and biological activities of silver nanoparticles synthesized using *Grewia tiliifolia* Vahl leaf extract, *Pharmaceut. Sci.* 29 (2022) 111–122.
- [56] N. Jaryal, H. Kaur, *Plumbago auriculata* leaf extract-mediated AgNPs and its activities as antioxidant, anti-TB and dye degrading agents, *Journal of Biomaterials science* 28 (2017) 1847–1858. *Polymer edition*.
- [57] R. Singh, L.U. Nawale, M. Arkile, U.U. Shedbalkar, S.A. Wadhvani, D. Sarkar, B.A. Chopade, Chemical and biological metal nanoparticles as antimycobacterial agents: a comparative study, *Int. J. Antimicrob. Agents* 46 (2015) 183–188.
- [58] K. Singh, S. Sharma, T. Banerjee, A. Gupta, S. Anupurba, Mutation detection and minimum inhibitory concentration determination against linezolid and clofazimine in confirmed XDR-TB clinical isolates, *BMC Microbiol.* 22 (2022) 1–8.
- [59] S. Wen, X. Gao, W. Zhao, F. Huo, G. Jiang, L. Dong, L. Zhao, F. Wang, X. Yu, H. Huang, Comparison of the in vitro activity of linezolid, tedizolid, sutezolid, and delpazolid against rapidly growing mycobacteria isolated in Beijing, China, *Int. J. Infect. Dis.* 109 (2021) 253–260.
- [60] M. Braback, K. Riesbeck, A. Forsgren, Susceptibilities of *Mycobacterium marinum* to gatifloxacin, gemifloxacin, levofloxacin, linezolid, moxifloxacin, telithromycin, and quinupristin-dalfopristin (Synercid) compared to its susceptibilities to reference macrolides and quinolones, *Antimicrob. Agents Chemother.* 46 (2002) 1114–1116.
- [61] V.K. Singh, K. Kavita, R. Prabhakaran, B. Jha, Cis-9-octadecenoic acid from the rhizospheric bacterium *Stenotrophomonas maltophilia* BJ01 shows quorum quenching and anti-biofilm activities, *Biofouling* 29 (2013) 855–867.
- [62] O.J. Oziri, Y. Wang, T. Watanabe, S. Uno, M. Maeki, M. Tokeshi, T. Isono, K. Tajima, T. Satoh, S.I. Sato, Y. Miura, PEGylation of silver nanoparticles by physisorption of cyclic poly (ethylene glycol) for enhanced dispersion stability, antimicrobial activity, and cytotoxicity, *Nanoscale Adv.* 4 (2022) 532–545.
- [63] B. Le Ouay, F. Stellacci, Antibacterial activity of silver nanoparticles: a surface science insight, *Nano Today* 10 (2015) 339–354.